Application of a Dung's Model to Predict Ductile Fracture of Aluminum Alloy Sheets Subjected to Deep Drawing

- **Hao Nguyen - Huu** [1]
- **Trung N. Nguyen** [2]
- **Hoa Vu - Cong** [1]

[1] Ho Chi Minh city University of Technology, VNU-HCM

[2] School of Mechanical Engineering, Purdue University, West Lafayette, IN 47907, USA

(Manuscript Received on August 01st, 2015, Manuscript Revised August 27th, 2015)

ABSTRACT:

In this paper, prediction of failed evolution of anisotropic voided ductile materials will be developed based on Dung's microscopic damage model. An isotropic and anisotropic formulation of the Dung's damage model that using von Mises yield criterion and Hill's quadratic anisotropic yield criterion (1948) integrated with isotropic hardening rules of matrix material used to simulate the deep drawing process of aluminum alloy sheets. The model is implemented as a vectorized user-defined material subroutine (VUMAT) in the ABAQUS/Explicit commercial finite element code. The predictions of ductile crack behavior in the specimens based on void nucleation, growth and coelescence are compared with Gurson – Tvergaard – Needleman (GTN) model and experiment results from reference.

Key words: *Ductile fracture, Sheet forming, Dung's model, Micro-crack mechanism, Anisotropy*.

1. INTRODUCTION

Recently, the aluminum alloy materials widely applied in automotive and aerospace industry since their light weight and excellent strength characteristics. The sheet metals made from aluminum alloys by rolling process is usually induced anisotropy. Therefore, investigation of plastic fractured behavior of these materials play an important role in industrial applications. The plastic micro-crack mechanism in the metal materials are based on assuming that matrix material contain inclusions and second phase particles. During matrix material under deformation then micro-crack will appear because of void nucleation, growth and coalescences. Gurson [1] proposed a yield function that isotropic matrix material contains spherical voids that including a special damage parameter of void volume fraction (f). Tvergaard [2, 3] modified the Gurson model by adding two adjusted parameters to consider interaction of the voids and hardening by deformation. Needleman and Tvergaard [4] extended Gurson model to simulate rapid loss of loading carrying capacity in the void materials. Therefore, Gurson model is also known as Gurson – Tvergaard – Needleman (GTN) model. Base on McClintock [5] spheroidal void growth model, Dung NL [6] investigated the cylindrical and elipsoidal void growth and then proposed a yield function similar to the yield function in GTN model but it has a hardening exponent (n). R. Schiffmann et al [7] used the Dung's void growth model to predict failure

development at ductile fracture of steel, it exhibited good agreement with experiment results. To determine void volume fraction growth during matrix material under deformation, Chu and Needleman [8] supplied the criterions for void nucleation into Gurson model. There is limit to anisotropic material of original porous plastic material model. Therefore, in recent years, some reseachers extended original Gurson model to anisotropic materials. Liao et al [9] integrated Gurson model with the Hill quadratic and non-quadratic anisotropic yield criteria to describe the matrix normal anisotropy and planar isotropy. Wang et el [10] formed a closed-form anisotropic Gurson yield criterion based on an average anisotropy parameter. Tanguy et al [11] developed a constitutive model based on Gurson model that integrating anisotropic behaviour and ductile damage for a X100 pipeline steel. Grange et al [12] predicted ductile fracture of Zircaloy-4 sheets based on the Gurson–Tvergaard–Needleman model which is extended to take into account plastic anisotropy and viscoplasticity. Chen and Dong [13] developed an implicit stress integration procedure to adapt the explicit dynamic solver for GTN model with equivalent stress is Hill's quadratic anisotropic yield criterion (1948). Morgeneyer et al [14] investigated fracture mechanisms of AA2139 Al-alloy sheet by experiments and GTN model to describe and predict deformation behaviour, crack propagation and toughness anisotropy.

Kami et al [15] predicted plastic fractue of AA6016-T4 metallic sheet of deep-drawing by using GTN model and Hill'48 quadratic anisotropic yield function.

In this paper, Dung's model based on Hill'48 expression of the equivalent stress is implemented by a VUMAT subroutine in the finite element software (ABAQUS) to investigate ductile fracture process of deep drawing in aluminum alloy materials. The predictions of ductile crack behavior in the specimens based on void nucleation, growth and coelescence are compared with GTN model and experiment results from referenced documents.

2. DUNG'S DAMAGE MODEL FOR ANISOTROPIC METAILLIC MATERIAL

Since original Dung's model constituted based on assume that matrix material is isotropy. Therefore, to apply the Dung's model on anisotropic material then von Mises equivalent stress in yield funtion will be replaced by Hill'48 quadratic anisotropic yield criterion.

The yield function of Dung's model [6]

$$\Phi=\left(\frac{\sigma_e}{\sigma_f}\right)^2+2fq_1\cosh\left[-\sqrt{3}(1-n)\frac{\sigma_m}{\sigma_f}\right]-1-(q_2 f)^2=0 \quad (1)$$

Where, the parameters q_1, q_2 are proposed by Tvergaard [4], n is hardening exponent of matrix material, hydrostatic stress $\sigma_m=-\frac{1}{3}\sigma_{ij}\delta_{ij}$, δ_{ij} is Kronecker delta, σ_e equivalent stress.

For von Mises yield criterion

$$\sigma_e=\sqrt{\frac{3}{2}\sigma'_{ij}:\sigma'_{ij}} \quad (2.1)$$

σ'_{ij} is deviatoric stress tensor

For Hill'48 equivalent stress[16].

$$\sigma_e=\Big[F(\sigma_{22}-\sigma_{33})^2+G(\sigma_{33}-\sigma_{11})^2+H(\sigma_{11}-\sigma_{22})^2+2L\sigma_{23}^2+2M\sigma_{31}^2+2N\sigma_{12}^2\Big]^{1/2} \quad (2.2)$$

σ_{ij} (i,j = 1, 2, 3) are Cartesian components of a Cauchy stress tensor. The parameters F, G, H, L, M and N are material constants. In the case of sheet metal material these parameters can be calculated by Lankford's coefficients.

$$F=\frac{r_0}{r_{90}\left(r_0+1\right)},\ G=\frac{1}{r_0+1},\ H=\frac{r_0}{r_0+1},$$
$$N=\frac{\left(r_0+r_{90}\right)\left(1+2r_{45}\right)}{2r_{90}\left(1+r_0\right)} \quad (3)$$

The Lankford's coefficients r_0, r_{45} and r_{90} are determined by unaxial tensile tests at 0°, 45° and 90° in rolling direction.

σ_f is the yield stress of matrix material.

$$\sigma_f=\sigma_f\left(\bar{\varepsilon}^p\right) \quad (4)$$

The equivalent plastic strain rate of matrix material $\dot{\bar{\varepsilon}}^p$ is dominated by equivalent plastic work:

$$\left(1-f\right)\sigma_f\dot{\bar{\varepsilon}}^p=\sigma_{ij}:\dot{\varepsilon}_{ij}^p \quad (5)$$

Where, $\bar{\varepsilon}^p$ is equivalent plastic strain of matrix material, $\dot{\varepsilon}_{ij}^p$ is plastic strain rate tensor.

The void volume fraction growth is computed as follow:

$$\dot{f}=\dot{f}_g+\dot{f}_n \quad (6)$$

Here, the void volume fraction growth of the presence voids in matrix material:

$$\dot{f}_g=\left(1-f\right)\dot{\varepsilon}_{ij}^p\delta_{ij} \quad (7)$$

The nucleated volume void fraction growth during matrix material under deformation:

$$\dot{f}_n=A\dot{\bar{\varepsilon}}^p \quad (8)$$

The number of nucleated voids A is a function of equivalent plastic strain of matrix material $\bar{\varepsilon}^p$:

$$A=\frac{f_N}{s_N\sqrt{2\pi}}\exp\left[-0.5\left(\frac{\bar{\varepsilon}^p-\varepsilon_N}{s_N}\right)^2\right] \quad (9)$$

Where, f_n, s_N, ε_N are the parameters relative to the void nucleation during matrix material under deformation.

3. NUMERICAL IMPLEMENTATION

A numerical algorithm based on the Euler backward method has been developed for a class of pressure-dependent plasticity models by Aravas [17] used to solve of the constitutive equations via a VUMAT subroutine in ABAQUS/Explicit software.

The steps of implementation procedures as follow:

Step1: Initialize the variables at initial time

$$\sigma_t,\varepsilon_t,f_t,\bar{\varepsilon}_t^p,\Delta\varepsilon_{t+\Delta t}$$

Step 2: Calculate trial state of stresses

Calculate stress tensor

$$\sigma_{t+\Delta t}^{el}=\sigma_t+D:\Delta\varepsilon_{t+\Delta t} \quad (10)$$

The fourth order tensor D is the elastic stiffness matrix. Isotropic elasticity is assumed so that

$$D_{ijkl}=\left(K-\frac{2}{3}G\right)\left(\delta_{ij}\delta_{kl}\right)+G\left(\delta_{ik}\delta_{jl}+\delta_{il}\delta_{jk}\right) \quad (11)$$

Where, K is the elastic bulk modulus, G is the shear modulus and δ_{ij} is the Kronecker delta

Calculate hydrostatic stress

$$\sigma_m^{el}=-\frac{1}{3}\sigma_{t+\Delta t}^{el}:I \quad (12)$$

Here, I is second order unit tensor

Calculate equivalent stress

$$\sigma_e^{el}=\sqrt{\frac{3}{2}\sigma_{ij}':\sigma_{ij}'} \quad (13.1)$$

Or

$$\sigma_e^{el}=\Big[F\left(\sigma_{22}-\sigma_{33}\right)^2+G\left(\sigma_{33}-\sigma_{11}\right)^2+H\left(\sigma_{11}-\sigma_{22}\right)^2+2L\sigma_{23}^2+2M\sigma_{31}^2+2N\sigma_{12}^2\Big]^{1/2} \quad (13.2)$$

Step 3: Check for plastic yield

$$\Phi^{trial}=\Phi\left(\sigma_m^{el},\sigma_e^{el},f_t,\bar{\varepsilon}_t^p\right)$$

If $\Phi^{trial}\le 0$ go to step 5 and update elastic stress, $\sigma_{t+\Delta t}=\sigma_{t+\Delta t}^{el}$

If $\Phi^{trial} > 0$ go to step 4 and calculate plastic correction.

Step 4: Calculate plastic correction

The plastic strain increment is divided into spherical and deviatoric parts:

$$\Delta\varepsilon^p = \frac{1}{3}\Delta\varepsilon_p I + \Delta\varepsilon_q n_{ij} \quad (14)$$

$$\Delta\varepsilon_p = -\lambda\frac{\partial\Phi}{\partial\sigma_m} \quad (15)$$

$$\Delta\varepsilon_q = \lambda\frac{\partial\Phi}{\partial\sigma_e} \quad (16)$$

λ is the plastic multiplier and $n_{ij} = (3/2\sigma_e)\sigma'_{ij}$ is the flow direction.

Eliminating λ from equations (15) and (16) leads to:

$$\Delta\varepsilon_q\left(\frac{\partial\Phi}{\partial\sigma_m}\right) + \Delta\varepsilon_p\left(\frac{\partial\Phi}{\partial\sigma_e}\right) = 0 \quad (17)$$

Using Newton-Raphson iterative method to solve the nonlinear system of equations (18) and (19), the consistency condition equation (20) must be met at the same time.

$$E_1 = \Delta\varepsilon_p^{(k+1)}\frac{\partial\Phi}{\partial\sigma_e} + \Delta\varepsilon_q^{(k+1)}\frac{\partial\Phi}{\partial\sigma_m} = 0 \quad (18)$$

$$E_2 = \Phi\left(\sigma_m^{(k+1)}, \sigma_e^{(k+1)}, \bar{\varepsilon}^{p(k+1)}, f^{(k+1)}\right) = 0 \quad (19)$$

$$\sigma_f^{(k+1)} = H^{(k+1)}\cdot\bar{\varepsilon}^p \quad (20)$$

Here, $H = \frac{d\sigma_f}{d\bar{\varepsilon}^p}$ is current strain hardening of the matrix material.

The algorithm stops iterations when the values of $|E_1|$ and $|E_2|$ are less than a specified tolerance δ = 1E-08

Step 5: Update of state variables

$$\sigma_m = \sigma_m^{el} + K\Delta\varepsilon_p \quad (21)$$

$$\sigma_e = \sigma_e^{el} - 3G\Delta\varepsilon_q \quad (22)$$

$$\sigma_{ij} = \sigma_{ij}^{el} - K\Delta\varepsilon_p I - 2G\Delta\varepsilon_q n_{ij} \quad (23)$$

$$\Delta\bar{\varepsilon}^p = \frac{-\sigma_m\Delta\varepsilon_p + \sigma_e\Delta\varepsilon_q}{(1-f)\sigma_f} \quad (24)$$

$$\Delta f = (1-f)\Delta\varepsilon_p + A\Delta\bar{\varepsilon}^p \quad (25)$$

4. NUMERICAL ANALYSIS

4.1. Tensile tests on single element

The subroutine is verified using a single 8-node brick element (C3D8R) for hydrostatic tensile test and plane strain element (CPE4R) for unaxial tensile test. The boundary conditions and loading as shown in figure 1. The initial size of each element edge is 1 mm. The loading velocity for tension is set to 15 mm/s.

The yield stress versus plastic strain rule:

$$\frac{\sigma_f}{\sigma_0} = \left(\frac{\sigma_f}{\sigma_0} + \frac{3G}{\sigma_0}\bar{\varepsilon}^p\right)^n \quad (26)$$

Where, σ_0 initial yield stress of matrix material, σ_0/E = 1/300, n = 0.1. The parameters of the porous plastic model: q_1 = q_2 = 1.5, initial void volume fraction f_0 = 0 and f_0 = 0.04 for strain plane and hydrostatic tension, respectively, ε_N = 0.3, s_N = 0.1, f_N = 0.04.

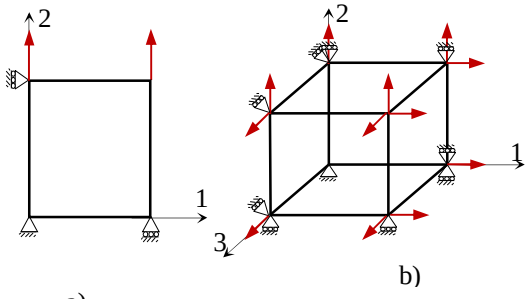

a) b)

Figure 1. Single element and boudary conditions: a) plane strain tension and b) hydrostatic tension

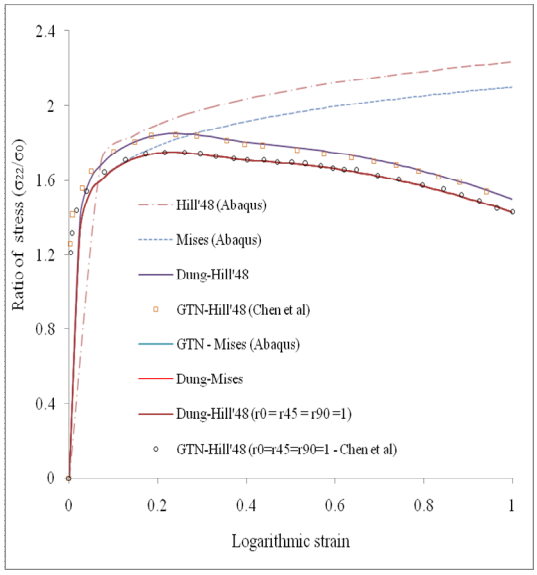

Figure 2. Uniaxial stress versus logarithmic strain in plane strain tension

Figure 2 shows ratio of stress (σ_{22}/σ_0) versus logarithmic strain $\varepsilon = ln(1+u/l_0)$. Where, u is the prescribed displacement and l_0 is the initial element length. In the case of isotropic material, Dung's model (Dung-Mises, Dung-Hill'48 with $r_0 = r_{45} = r_{90} = 1$) concides with results of GTN model in Abaqus (GTN-Mises) and Chen et al [13] (GTN Hill'48 $r_0 = r_{45} = r_{90} = 1$). In the case of anisotropic material, Dung's model (Dung-Hill'48) presents very good agreement with result of Chen [13] (GTN-Hill'48 – Chen et al).

For yield function without damage variable (Hill'48 and von Mises), axial stress greater than Dung's model and GTN model due to damage gradually accumulates by void volume fraction (f) in porous plastic material model.

Figure 3 prensents void volume fraction growth in deformation of matrix material. For isotropic material Dung's model (Dung-Mises, Dung-Hill'48, $r_0 = r_{45} = r_{90} = 1$) concides with GTN model in Abaqus. For anisotropic material, void volume fraction of Dung's model (Dung-Hill'48) lower a little because of Lankford's coefficients.

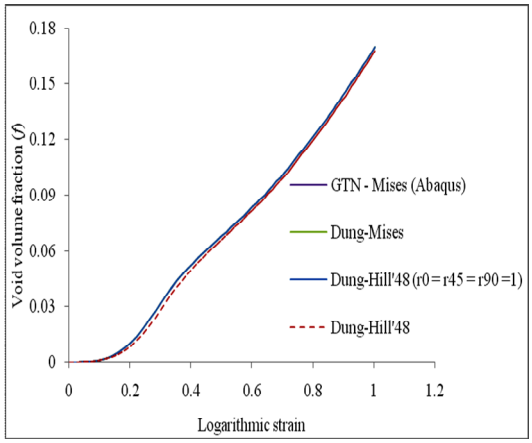

Figure 3. Void volume fraction versus logarithmic strain in plane strain tension

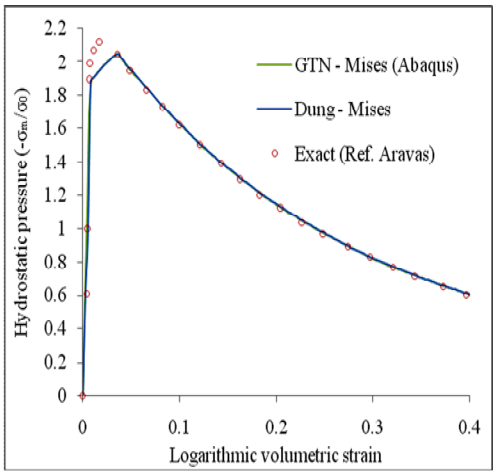

Figure 4. Hydrostatic stress versus logarithmic volumetric strain in hydrostatic tension

In figure 4, the hydrostatic stress is plotted as a function of logarithmic volumetric strain $\varepsilon_v = 3ln(1+u/l_0)$. Figure 5 shows void volume fraction as a function of logarithmic volumetric strain. The Dung's model agree very well with GTN model in Abaqus and excact solution of N. Aravas [18]

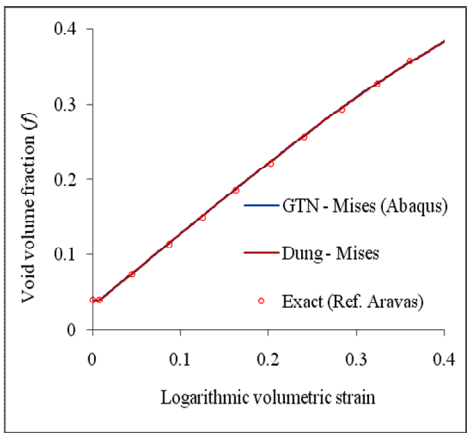

Figure 5. Void volume fraction versus logarithmic volumetric strain in hydrostatic tension

4.2. Deep drawing

In this section, cylindrical cup and square cup deep drawing process was be investigated. The forming behavior of Dung's damage model was compared with GTN model in Abaqus and experiment results from refercences.

4.2.1. Cylindrical cup deep drawing

The material of sheet is AA6111-T4 aluminum alloy. The properties of porous material is refered to Chen et al [13] as table 1.

Table 1. Damage parameters of AA6111-T4 aluminum alloy for Dung's model

f_0	ε_N	f_N	s_N	f_c	q_1	q_2
0.0	0.3	0.04	0.1	0.15	1.5	1.5

The isotropic hardening rule of matrix material:

$$\sigma_f = \sigma_0 + a\left(1 - e^{-b\bar{\varepsilon}^p}\right) \quad (27)$$

Here, σ_f is the equivalent stress of matrix material, $\bar{\varepsilon}^p$ is the equivalent plastic strain, σ_0 is the initial yield stress, a and b are the material constants. The material properties of AA6111-T4 alloy in the unxiaxial tensile test as table 2. Figure 6 shows tooling setup for cylindrical cup drawing. The sheet thickness is 1 mm. The punch stroke is 50 mm. The blank holding force is 50 kN. Element type of blank is eight-node linear brick, reduced integration with hourglass control continuum element (C3D8R). The rigid element (R3D4) of tools is chosen. The friction coefficient has been set to a value of 0.0096 on all the contact surfaces.

Table 2. The material properties of AA6111-T4 aluminum alloy [13]

E(GPa)	*v*	σ_0*(MPa)*	r_0	r_{45}	r_{90}	*a(MPa)*	*b*
70.5	0.342	180.8	0.894	0.611	0.66	274.64	6.79

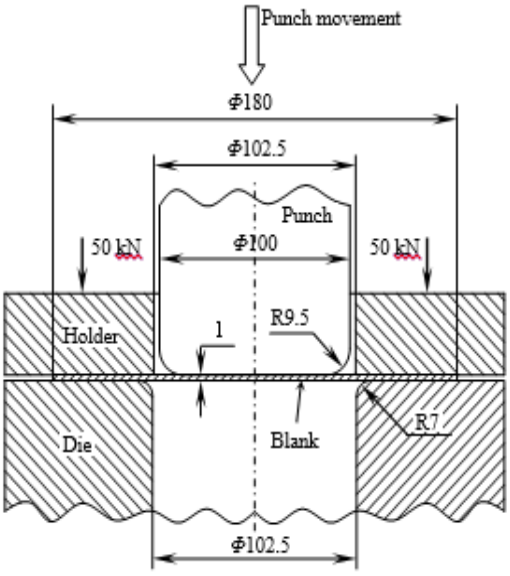

Figure 6. Tooling setup for cylindrical cup drawing in NUMISHEET'2002 (unit: mm)

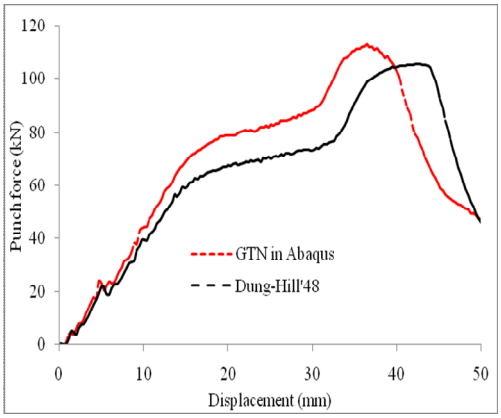

Figure 7. Punch force versus punch displacement

In the figure 7, punch force is plotted as a function of punch displacement. The Dung-Hill'48 anisotropic plastic damage model is a little smaller than that by GTN model in Abaqus.

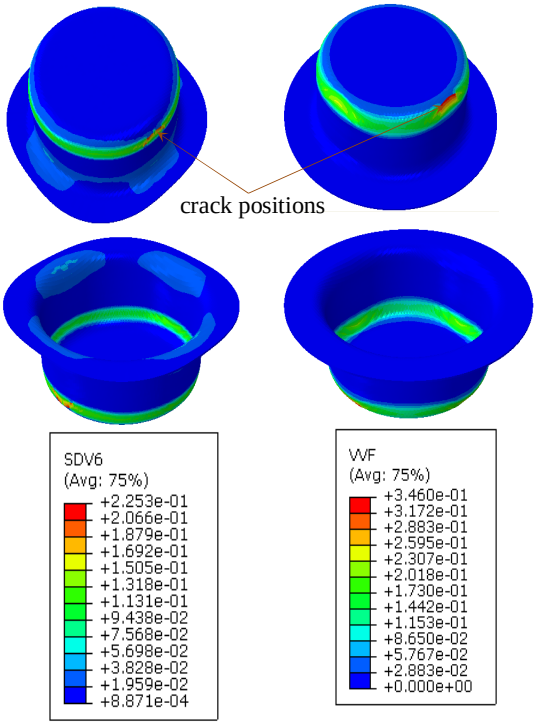

a) b)

Figure 8. Distribution of void volume fraction: a) anisotropic plastic damage model (Dung-Hill'48) and b) isotropic plastic damage model (GTN in Abaqus)

Figure 8 shows comparison of distribution of void volume fraction between Dung-Hill'48 model and GTN model in Abaqus at depth 45 mm of punch stroke. For Dung-Hill'48, material displays anisotropy strongly by earing phenomenon.

4.2.2. Square cup deep drawing

The AA6016-T4 aluminum alloy sheet was used to predict plastic fracture in deep drawing process. The parameters of damage model given in table 3.

Table 3. Damage parameters of AA6016-T4 aluminum alloy for Dung's model [15]

f_0	ε_N	f_N	s_N	f_c	f_F	q_1	q_2
2.4e-4	0.3	0.041546	0.1	0.047674	0.2	1.5	1.5

The yield stress versus plastic strain curve that fitting from experiment data in tensile test of AA6016-T4 aluminum alloy by means of Swift's hardening rule:

$$\sigma_f = A\left(\varepsilon_0 + \bar{\varepsilon}^p\right)^n \qquad (28)$$

The material properties as table 4

Table 4. The material properties of AA6016-T4 aluminum alloy [15]

$E(GPa)$	v	$A(MPa)$	r_0	r_{45}	r_{90}	$\varepsilon_0(MPa)$	n
70	0.33	525.77	0.5529	0.4091	0.5497	0.01125	0.27

The deep drawing tools was installed as figure 9. The diameter of circular blank is 85 mm. The holding force is 10 kN. Punch stroke is 25 mm.

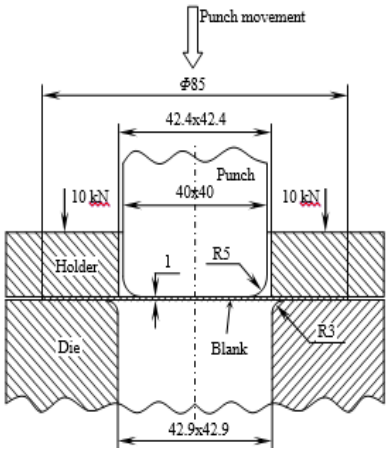

Figure 9. Diagram of the tooling setup in square cup drawing (unit: mm) [19]

The rigid shell elements (R3D4) was used to mesh punch, die and blank holder, while 8-node hexahedral (C3D8R) solid elements have been meshed blank. The size of initial length of element is 0.5 mm. The friction coefficient has been set to a value of 0.05 on all the contact surfaces.

Figure 10 compares fracture shape of specimens between simulated results and experiment of Kami et al [15]. The image show the failed path and position of Dung's model that based on equivalent stress of Hill (1948) is smilar to experiment.

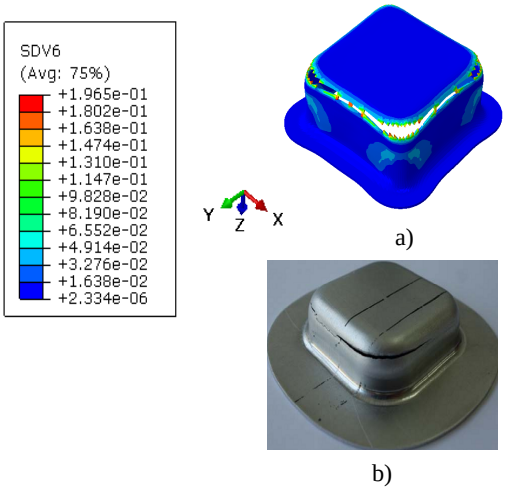

Figure 10. Failed specimens: a) Dung-Hill'48 and b) experiment [15].

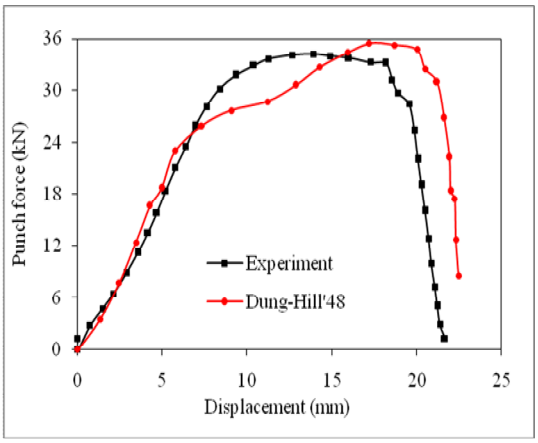

Figure 11. Comparion of forming forces for blank holder of 10 kN

Figure 11 shows comparison of punch force versus displacement curve between Dung's model and experiment of Kami et al [15]. The maximum values of punch force are 35.28 kN and 34.24 kN for Dung's model and experiment result, respectively. The punch force towards zero at 20.03 mm of depth is predicted by Dung's model, while that experiment data is 18.7 mm, it is acceptable.

5. CONCLUSIONS

In this paper, the Dung's model is implemented using the commercial code Abaqus/Explicit with the user-difined material subroutine (VUMAT).

The subroutine is verified via the simple finite element models of plane strain and hydrostatic tension. The analysis results based on Dung's model have been compared to the GTN model in Abaqus and the results from literature. It is shown that the Dung's model is capacable of predicting damage localization of metallic material.

The two deep drawing processes of the cylindrical cup and square cup have been simulated. For the first case, fracture positions of Dung's model is similar to the GTN model in Abaqus, but it includes a little earing phenomenon and forming force is smaller. In the case of square cup deep drawing, comparison with the experimentally indicated very identical crack path. It is shown that the forming force and the deep displacement of punch that the punch force toward zero of Dung's model are higher than that by experiment result with an acceptable accuracy.

Ứng dụng mô hình của Dũng để dự đoán phá hủy dẻo của tấm hợp kim nhôm trong quá trình dập sâu

- **Nguyễn Hữu Hào** [1]
- **Trung N. Nguyen** [2]
- **Vũ Công Hòa** [1]

[1] Trường Đại học Bách Khoa, ĐHQG-HCM

[2] Trường Cơ khí, Đại học Purdue, West Lafayette, IN 47.907, USA

TÓM TẮT:

Bài báo trình bày sự dự đoán quá trình phá hủy dẻo trong vật liệu kim loại bất đẳng hướng dựa trên mô hình phá hủy vi mô của Nguyễn Lương Dũng. Mô hình phá hủy của Dũng sẽ được kết hợp với tiêu chuẩn chảy cho vật liệu đẳng hướng von Mises và tiêu chuẩn chảy cho vật liệu bất đẳng hướng Hill'48 cùng với các hàm biến cứng đẳng hướng của vật liệu để dự đoán nứt dẻo trong quá trình dập sâu tấm hợp kim nhôm. Mô hình được lập trình bằng một chương trình vật liệu do người dùng tự định nghĩa (VUMAT) trong gói phần mềm phần tử hữu hạn Abaqus/Explicit. Các dự đoán ứng xử nứt dẻo trong các mẫu dựa vào các tham số tạo mầm, tăng trưởng và liên kết lỗ hổng vi mô trong vật liệu mạng sẽ được so sánh với mô hình Gurson-Tvergaard-Needleman (GTN) trong Abaqus và các kết quả thí nghiệm tham khảo từ các công bố quốc tế.

Từ khóa: *Nứt dẻo, Gia công tấm, Mô* hình *của Dũng, Cơ chế nứt vi mô, Bất đẳng hướng.*

REFERENCES

[1]. Gurson, A. L. Continuum Theory of Ductile Rupture by Void Nucleation and Growth: Part I—Yield Criteria and Flow Rules for Porous Ductile Media. *Journal of Engineering Materials and Technology*, 99, 1 1977), 2-15.

[2]. Tvergaard, V. On localization in ductile materials containing spherical voids. *Int J Fract*, 18, 4 (1982/04/01 1982), 237-252.

[3]. Tvergaard, V. Influence of voids on shear band instabilities under plane strain conditions. *Int J Fract*, 17, 4 (1981/08/01 1981), 389-407.

[4]. Tvergaard, V. and Needleman, A. Analysis of the cup-cone fracture in a round tensile bar. *Acta Metallurgica*, 32, 1 (1// 1984), 157-169.

[5]. McClintock, F. A. A Criterion for Ductile Fracture by the Growth of Holes. *Journal of Applied Mechanics*, 35, 2 1968), 363-371.

[6]. Dung, N. L. Three Dimensional Void Growth in Plastic Materials. *Mechanics Research Comunications*, 19, 3 1992), 227.

[7]. Schiffmann, R., Wendt, U. and Dahl, W. Damage mechanical investigations at ductile fracture of free-cutting steels by means of

microscopy-void growth and fracture surface topography. *Le Journal de Physique IV*, 11, PR5 2001), Pr5-187-Pr185-193.

[8]. Chu, C. C. and Needleman, A. Void Nucleation Effects in Biaxially Stretched Sheets. *Journal of Engineering Materials and Technology*, 102, 3 1980), 249-256.

[9]. Liao, K. C., Pan, J. and Tang, S. C. Approximate yield criteria for anisotropic porous ductile sheet metals. *Mechanics of Materials*, 26, 4 (12// 1997), 213-226.

[10]. Wang, D.-A., Pan, J. and Liu, S.-D. An anisotropic Gurson yield criterion for porous ductile sheet metals with planar anisotropy. *International Journal of Damage Mechanics*, 13, 1 2004), 7-33.

[11]. Tanguy, B., Luu, T. T., Perrin, G., Pineau, A. and Besson, J. Plastic and damage behaviour of a high strength X100 pipeline steel: Experiments and modelling. *International Journal of Pressure Vessels and Piping*, 85, 5 (5// 2008), 322-335.

[12]. Grange, M., Besson, J. and Andrieu, E. An anisotropic Gurson type model to represent the ductile rupture of hydrided Zircaloy-4 sheets. *Int J Fract*, 105, 3 (2000/10/01 2000), 273-293.

[13]. Chen, Z. and Dong, X. The GTN damage model based on Hill'48 anisotropic yield criterion and its application in sheet metal forming. *Computational Materials Science*, 44, 3 (1// 2009), 1013-1021.

[14]. Morgeneyer, T. F., Besson, J., Proudhon, H., Starink, M. J. and Sinclair, I. Experimental and numerical analysis of toughness anisotropy in AA2139 Al-alloy sheet. *Acta Materialia*, 57, 13 (8// 2009), 3902-3915.

[15]. Kami, A., Mollaei Dariani, B., Sadough Vanini, A., Comsa, D.-S. and Banabic, D. Application of a GTN damage model to predict the fracture of metallic sheets subjected to deep-drawing. *Proceedings of the Romanian Academy, Series A*, 152014), 300-309.

[16]. Hill, R. *A theory of the yielding and plastic flow of anisotropic metals*. The Royal Society, City, 1948.

[17]. Aravas, N. On the numerical integration of a class of pressure-dependent plasticity models. *International Journal for Numerical Methods in Engineering*, 24, 7 1987), 1395-1416.

[18]. Aravas, N. On the numerical integration of a class of pressure-dependent plasticity models. *International Journal for numerical methods in engineering*, 24, 7 1987), 1395-1416.

[19]. Nicodim, I., Ciobanu, I. and Banabic, D. Effect of the constitutive law on the prediction of the wall thickness distribution of square cup2013).